ACS central science

Research Article

Cite This: ACS Cent. Sci. 2019, 5, 524−538

http://pubs.acs.org/journal/acscii

Molecular Basis of Broad Spectrum *N*-Glycan Specificity and Processing of Therapeutic IgG Monoclonal Antibodies by Endoglycosidase S2

Erik H. Klontz,[†,‡,§,¶] Beatriz Trastoy,[∥,¶] Daniel Deredge,[⊥] James K. Fields,[†,‡,§] Chao Li,[#] Jared Orwenyo,[#] Alberto Marina,[∥] Robert Beadenkopf,[†] Sebastian Günther,[†,▽] Jair Flores,[†] Patrick L. Wintrode,[⊥] Lai-Xi Wang,[#] Marcelo E. Guerin,*[,∥,○] and Eric J. Sundberg*[,†,‡,◆]

[†]Institute of Human Virology, [‡]Department of Microbiology & Immunology, and [§]Program in Molecular Microbiology & Immunology, University of Maryland School of Medicine, Baltimore, Maryland 21201, United States

[∥]Structural Biology Unit, CIC bioGUNE, Bizkaia Technology Park, 48160 Derio, Spain

[⊥]Department of Pharmaceutical Sciences, University of Maryland School of Pharmacy, Baltimore, Maryland 21201, United States

[#]Department of Chemistry and Biochemistry, University of Maryland, College Park, Maryland 20742, United States

[▽]Photon Science, Deutsches Elektronen-Synchrotron, Hamburg 22607, Germany

[○]IKERBASQUE, Basque Foundation for Science, 48013 Bilbao, Spain

[◆]Department of Medicine, University of Maryland School of Medicine, Baltimore, Maryland 21201, United States

Supporting Information

ABSTRACT: Immunoglobulin G (IgG) glycosylation critically modulates antibody effector functions. *Streptococcus pyogenes* secretes a unique endo-*β*-*N*-acetylglucosaminidase, EndoS2, which deglycosylates the conserved *N*-linked glycan at Asn297 on IgG Fc to eliminate its effector functions and evade the immune system. EndoS2 and specific point mutants have been used to chemoenzymatically synthesize antibodies with customizable glycosylation for gain of functions. EndoS2 is useful in these schemes because it accommodates a broad range of *N*-glycans, including high-mannose, complex, and hybrid types; however, its mechanism of substrate recognition is poorly understood. We present crystal structures of EndoS2 alone and bound to complex and high-mannose glycans; the broad *N*-glycan specificity is governed by critical loops that shape the binding site of EndoS2. Furthermore, hydrolytic experiments, domain-swap chimeras, and hydrogen−deuterium exchange mass spectrometry reveal the importance of the carbohydrate-binding module in the mechanism of IgG recognition by EndoS2, providing insights into engineering enzymes to catalyze customizable glycosylation reactions.

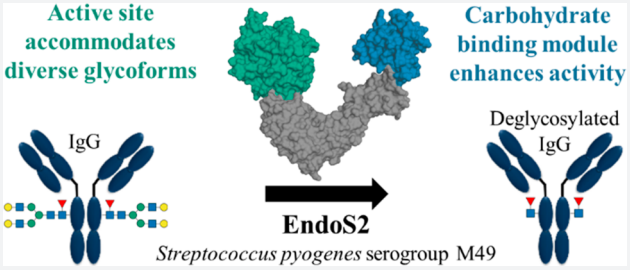

INTRODUCTION

Antibodies are a foundation of the human immune system, protecting us from cancer and infectious diseases. A glycosylation site on Asn297 of the fragment crystallizable (Fc) domain of immunoglobulin G (IgG) antibodies critically modulates the effector functions of antibodies.[1] The obligate human pathogen *Streptococcus pyogenes* secretes at least two endoglycosidases with different *N*-glycan specificities that allow the bacterium to remove more than 20 glycoforms from antibodies, eliminating their effector functions to evade the immune system.[2,3] The best characterized of these enzymes is EndoS, an endo-*β*-*N*-acetylglucosaminidase that hydrolyzes biantennary complex-type (CT) *N*-glycans from IgG between the first two *N*-acetylglucosamine (GlcNAc) residues.[2,4] EndoS has been investigated in numerous applications: as a therapy for antibody-mediated autoimmune diseases, such as systemic lupus erythematosus, epidermolysis bullosa acquisita, and idiopathic thrombocytopenia purpua;[5−8] as an enhancer of monoclonal antibody therapy;[9] as a tool for the chemoenzymatic synthesis of antibodies with homogeneous glycosylation or drug conjugates;[10−12] and as a method to screen for chronic inflammatory disease states.[13] Another *Streptococcus pyogenes* antibody-disrupting enzyme, IdeS, cleaves antibodies in their hinge region, and has shown promise in clinical trials for reducing antibody-mediated organ transplant rejection, revealing yet another possible application for endoglycosidases.[14]

It was recently discovered that *Streptococcus pyogenes* serogroup M49 secretes a unique endoglycosidase, EndoS2, which may offer several potential therapeutic and biotechnological advantages compared to EndoS. EndoS2 has a broader

Received: December 10, 2018
Published: February 6, 2019

DOI: 10.1021/acscentsci.8b00917
ACS Cent. Sci. 2019, 5, 524−538

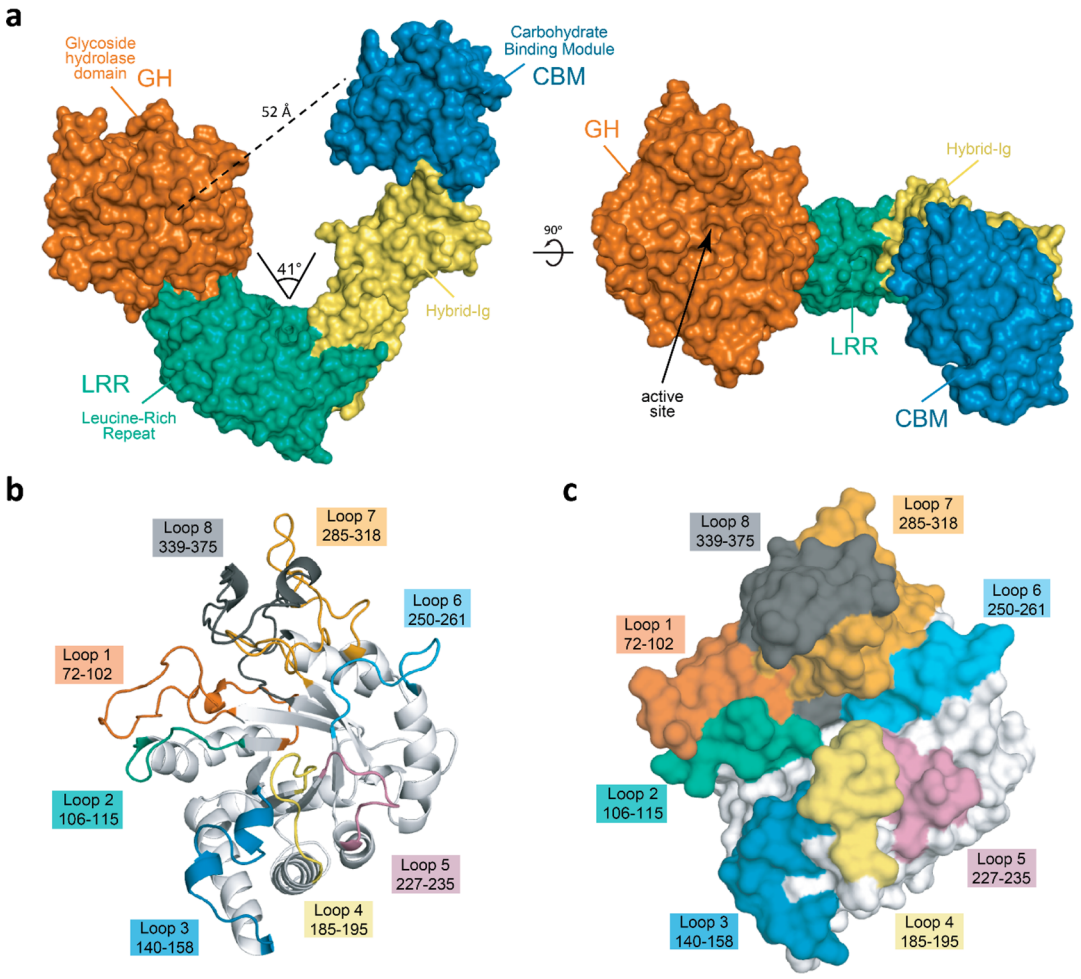

Figure 1. Overall architecture of EndoS2. (a) Overall structure of EndoS2 with annotated domains. The annotated distance is measured from the Cα of a conserved catalytic glutamate in the GH domain (E186) to the Cα of a conserved tryptophan in the CBM (EndoS2 W712). The annotated angle is between these two residues and the Cα of the first residue in the hybrid-Ig domain, near the base of the hinge (E548). (b) Cartoon and (c) surface representations showing the overall topology and annotation of GH domain loops.

substrate glycan specificity, hydrolyzing not only biantennary CT *N*-glycans, but also high-mannose (HM), hybrid, and bisecting CT *N*-glycans on IgG.[3] The chemical structure and heterogeneity of the *N*-linked glycans significantly impact the efficacies, stabilities, and effector functions of antibodies.[15] A strategy to better control their therapeutic properties is the chemoenzymatic synthesis of homogeneously *N*-glycosylated antibodies using endoglycosidases, glycosynthases, and *N*-glycan oxazolines.[4,11,16] In this regard, glycosynthase mutants of EndoS2 have been developed to engineer antibodies with a more diverse set of *N*-glycans than similar EndoS mutants are capable of creating.[17] By recognizing more IgG *N*-glycans, EndoS2 may also prove itself superior to EndoS in the treatment of autoimmune diseases. EndoS2 is also interesting because of its narrow protein specificity, recognizing intact IgG and α_1-acid glycoprotein (AGP), but not a host of other proteins, including α_2-macroglobulin, ovalbumin, lactoferrin, RNase B, fetuin, denatured IgG, and denatured AGP.[3] Despite the myriad potential uses of EndoS2 in monitoring and treating human diseases, its molecular mechanism of substrate recognition is poorly understood.

Our recent structural analyses of EndoS, however, have revealed how this enzyme recognizes its CT substrate on IgG antibodies.[18,19] EndoS forms a "V" shape, with a GH18 chitinase domain that contains the active site on one tip of the "V" and a carbohydrate-binding module (CBM) on the other tip. We previously showed in EndoS that a subset of active site loops form the main determinants of substrate binding by creating contacts with the pentasaccharide core and $\alpha(1-3)$ antenna of biantennary CT glycans.[18] The CBM of EndoS has been shown to bind D-galactose,[20] and single point mutants can eliminate IgG binding and catalysis; however, little else is known about the role of this domain.[19] Carbohydrate-binding modules are noncatalytic domains that are frequently appended to carbohydrate active enzymes. They can assist catalysis in many ways, such as by binding to carbohydrates to increase their local concentration, or by disrupting tightly packed carbohydrates to increase their accessibility by the catalytic GH domain.[21]

EndoS2 is predicted to have a GH18 domain and CBM; how these two domains contribute to its specificities, though, is unknown. Here, we present X-ray crystal structures of EndoS2, both alone and bound to CT and HM substrates. The latter structure is the first instance of an endo-β-*N*-acetylglucosaminidase with a HM-glycan bound and helps reveal the molecular mechanism of EndoS2 *N*-glycan recognition. Our results also provide mechanistic insight into the role of the CBM in substrate recognition and lay the foundation for how these

DOI: 10.1021/acscentsci.8b00917
ACS Cent. Sci. 2019, 5, 524−538

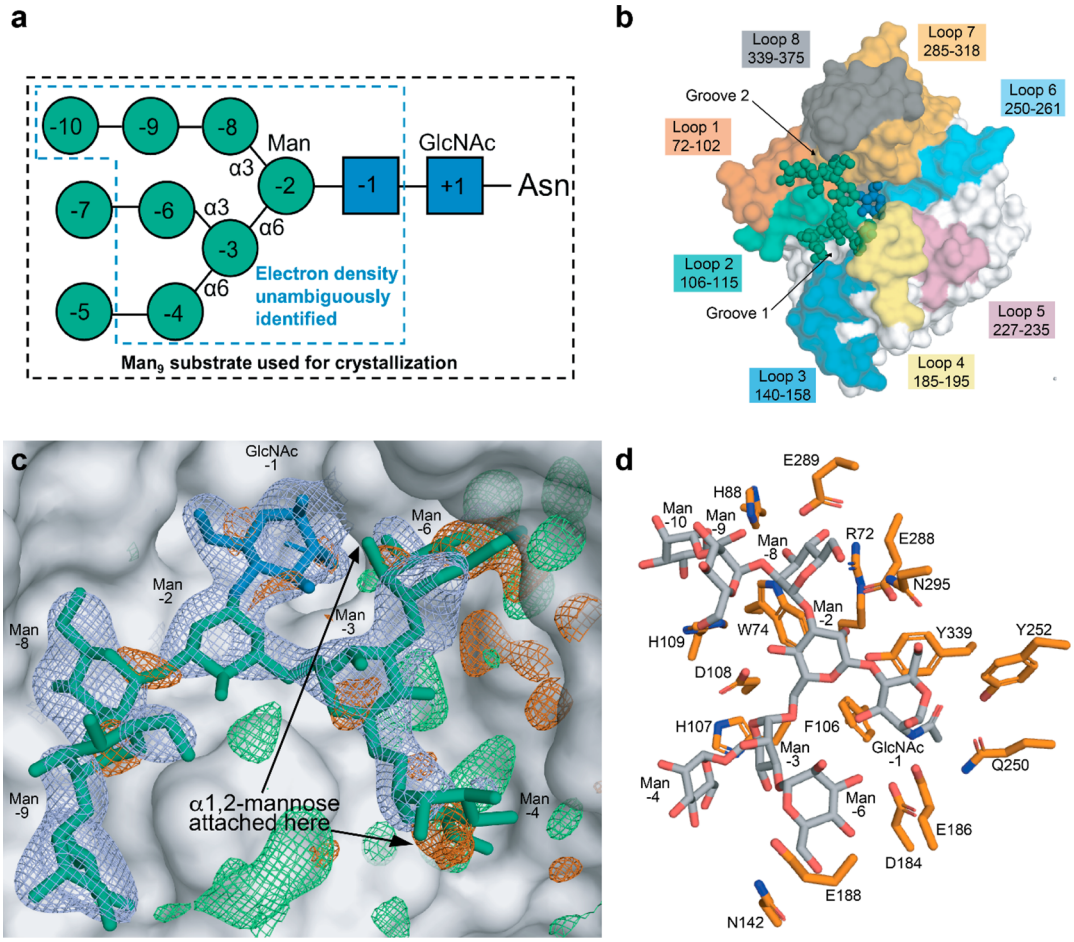

Figure 2. Crystal structure of EndoS2 with high-mannose glycan. (a) Structure of a high-mannose (man_9) *N*-glycan, with annotations for the parts used for crystallization (black box), and the parts unambiguously identified in the crystal structure (blue box). (b) Overall structure of the glycan bound within the active site crevasse of the GH domain. Annotation of GH domain loops for EndoS2 is colored. (c) Composite omit map of electron density surrounding the high-mannose glycan: blue mesh, 2Fo-Fc contoured to 1σ, carved to 1.8 Å surrounding the full glycan; green mesh, positive density (Fo−Fc) contoured to 3σ, carved to 5 Å surrounding the α6 antenna; red mesh, negative density (Fo−Fc) contoured to 3σ, carved to 5 Å surrounding the α6 antenna. Arrows indicate the attachment sites for the remaining two mannose residues. (d) Key residues of EndoS2 interacting with HM product are colored in orange.

domains can be incorporated into strategies to engineer enzymes with novel functions.

RESULTS

Overall Structure of Full-Length EndoS2. The crystal structures of full-length wild-type EndoS2 in its unliganded form, and in complex with HM and CT substrates, were solved by molecular replacement at 2.75, 2.50, and 2.50 Å resolution, respectively (Figure 1, Table S1). EndoS2 crystallized in the $P2_12_12_1$ space group with two molecules per asymmetric unit. The structures reveal that EndoS2 is a monomeric "V-shaped" protein, composed of four different domains from N- to C-terminus: (i) a glycoside hydrolase (GH) domain (residues 43−386); (ii) a leucine-rich repeat (LRR) domain (residues 387−547); (iii) a hybrid-Ig domain (residues 548−680); and (iv) a carbohydrate-binding module (CBM; residues, 681−843). The "V-shape" of EndoS2 measures ∼102 Å across and ∼81 Å high, with a tapered cleft measuring ∼35 Å across its opening, with active site located in the GH domain on one tip of the "V", and the CBM on the other tip (Figure 1a). EndoS2 belongs to the family 18 of glycoside hydrolases (GH18),[3] comprising a group of enzymes that contains both chitinases (EC 3.2.1.14), with hydrolytic activity on chitin, and endo-β-*N*-acetylglucosaminidases (EC 3.2.1.96), with endoglycosidase activity on the chitobiose core of *N*-linked complex glycans.[22]

Structural Basis of High-Mannose-Type *N*-Glycan Recognition by EndoS2. The EndoS2 GH domain adopts an $(\alpha/\beta)_8$-barrel topology typical of GH18 family enzymes. The GH domain contains several loops that connect the α-helices and β-strands, shaping a long cavity in which the *N*-glycans bind (Figure 1b,c), including β1−β2 (loop 1; residues 72−102), β2−α2 (loop 2; residues 106−115), β3−α3 (loop 3; residues 140−158), β4−α4 (loop 4; residues 185−195), β5−α5 (loop 5; residues 227−235), β6−α6 (loop 6; residues 250−261), β7−α7 (loop 7; residues 285−318), and β8−α8 (loop 8; residues 339−375). To understand the unique features of EndoS2 that allow it to recognize HM *N*-glycans, we solved the crystal structure of EndoS2 into which a full-size HM-type *N*-glycan, $Man_9GlcNAc_2Asn$, was soaked (EndoS2-HM; Figure 2a, Table S1). The HM-glycan binds in the crevasse within the GH domain (Figure 2b). Electron density unambiguously identified 7 out of the 9 mannose residues and one GlcNAc residue in the crystal structure ($Man_7GlcNAc_1$; Figure 2c). The full α(1,3) antenna could be easily resolved in a single conformation, potentially identifying these contacts as being more important in the binding mechanism of HM. In

DOI: 10.1021/acscentsci.8b00917
ACS Cent. Sci. 2019, 5, 524−538

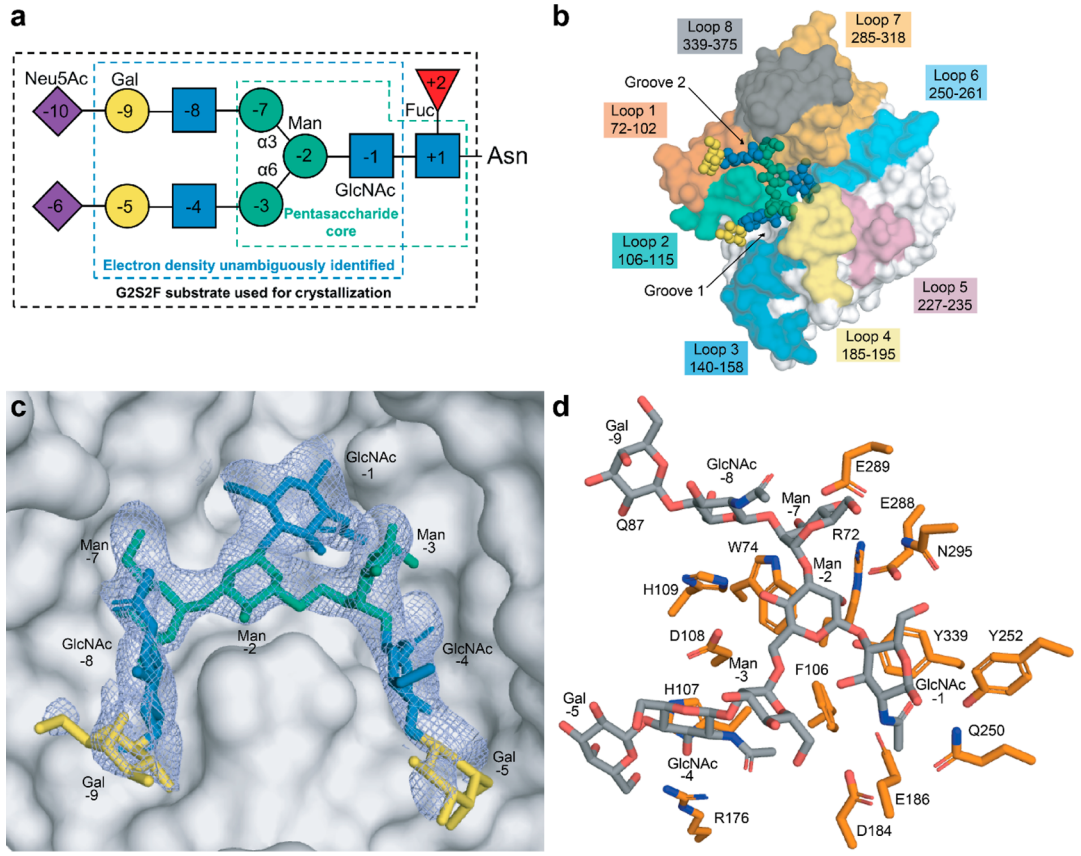

Figure 3. Crystal structure of EndoS2 with complex biantennary glycan. (a) Structure of a full complex biantennary glycan, with annotations for the parts used for crystallization (black box), the parts unambiguously identified in the crystal structure (blue box), and the pentasaccharide core (green box). (b) Overall structure of the glycan bound within the active site crevasse of the GH domain. Annotation of GH domain loops for EndoS2 is colored. (c) Blue mesh illustrates the composite omit map of electron density (2Fo−Fc) contoured to 1σ and carved to 1.8 Å surrounding the CT glycan. (d) Key residues of EndoS2 interacting with CT product are colored in orange.

contrast, although a composite omit map shows substantial positive (Fo−Fc) density remaining near the location where the last two mannose residues of the α(1,6) antenna should be, we could not reliably model them in just one or a few discrete positions, suggesting that the α(1,6) antenna samples a broad distribution of conformations. The conformation of the enzyme does not change upon binding of the HM-glycan, with an overall RMSD (root-mean-square deviation) value of 0.74 Å for the main chain atoms of the liganded and unliganded EndoS2. The reducing end of the core Manβ1−4GlcNAc is located above the central area of the β-barrel, forming contacts with loops 2, 4, 6, 7, and 8. GlcNAc (−1) is adjacent to the two conserved catalytic residues of this family of enzymes.[23−27] The binding pocket is formed by two grooves that accommodate the α(1,6) antenna (groove 1) and the α(1,3) antenna (groove 2) of the HM-glycan. Specifically, the O1 and oxygen and nitrogen of the 2-acetamido group of the GlcNAc (−1) form hydrogen bonds with the side chains of E186, Y252, and D184, respectively (Figure 2d, Figure S1). These interactions stabilized the GlcNAc (−1) in a "skew-boat" conformation, the enzyme−product complex formed after the nucleophilic attack of a water molecule and before the release of the final product (Figure S2). A similar conformation has been observed in other crystal structures of enzymes of the GH18 family in complex with their products,[28−33] suggesting it might be part of the conformational itinerary of the sugar residue along the catalytic cycle.[34,35] This was made possible by the short soaking time (ca. 1 min) used to obtain this structure, which allows the GlcNAc (+1) to be released, as made evident by the absence of electron density for it. In addition, the O6 of the GlcNAc (−1) makes a hydrogen bond with the side chain of N295. The O2 of Man (−2) hydrogen bonds with residues E288 and Y339, while O4 interacts with D108. The carbohydrate moieties of the α(1,6) antenna barely make contacts with residues in the loops that decorate the binding pocket, in contrast with those of the α(1,3) antenna. For instance, O3 and O4 of Man (−8) hydrogen bonds with the side and main chain of E289, respectively, and O6 of Man (−8) hydrogen bonds with the side chain of N295. Furthermore, the ring-oxygen of Man (−9) and O5 of Man (−10) form hydrogen bonds with the side chains of H109 and H88, respectively. The bottom of the binding pocket is built up by hydrophobic residues, Y70, Y339, and F109, which pack against GlcNAc (−1). Y339 and F109 interact with Man (−2) whereas R72 and W74 interact with Man (−8) (Figure 2d, Figure S1).

Structural Basis of Complex-Type *N*-Glycan Recognition by EndoS2. To understand the molecular basis for complex-type *N*-glycan recognition by EndoS2, we solved the X-ray cocrystal structure of the enzyme bound to a CT glycan [specifically G2S2, which bears a galactose and sialic acid at the nonreducing end of each antenna (EndoS2-CT; Figure 3a, Table S1)]. As expected, this CT glycan was found to bind in the same crevasse as the HM-glycan (Figure 3b). Although a

DOI: 10.1021/acscentsci.8b00917
ACS Cent. Sci. 2019, 5, 524−538

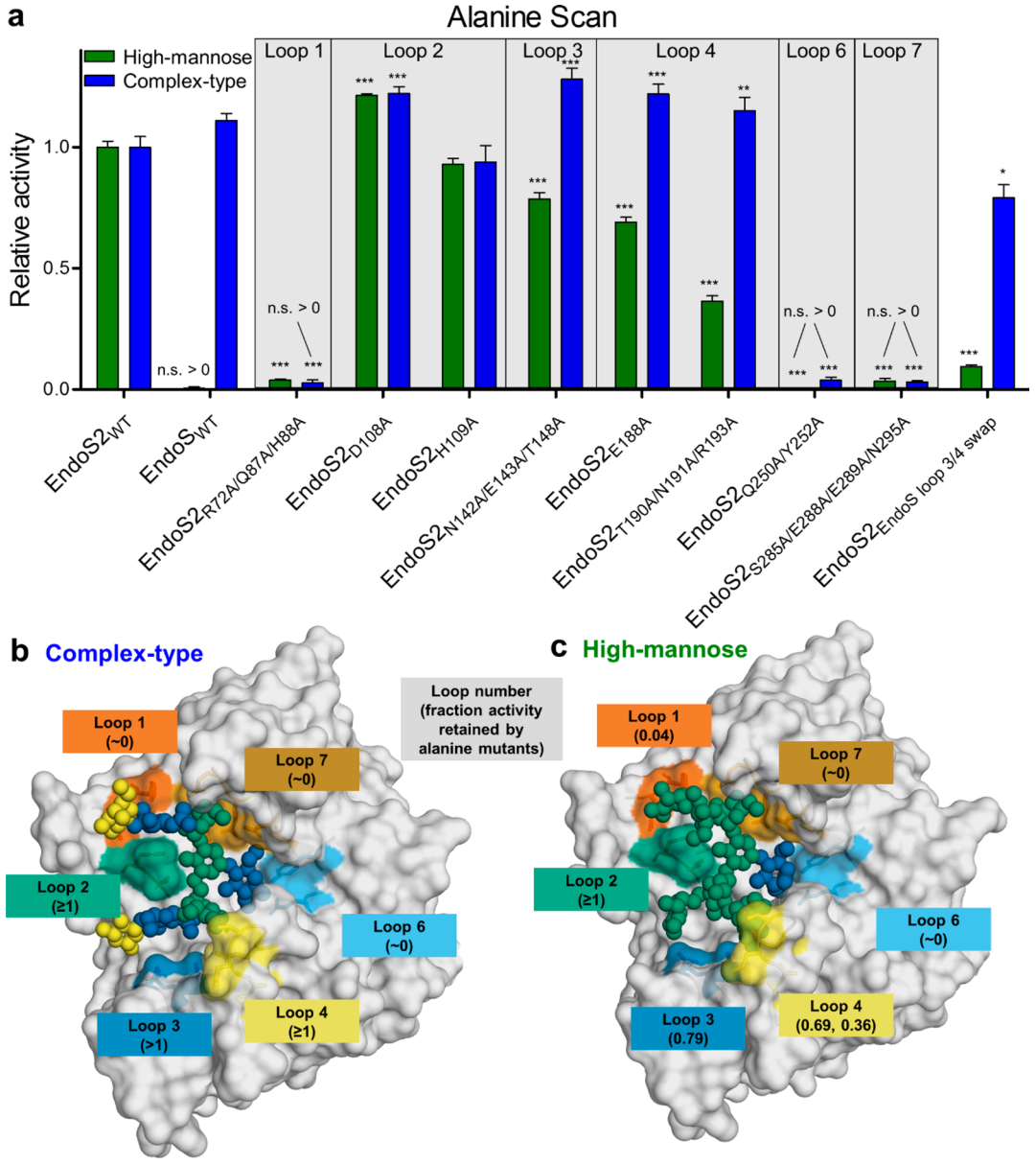

Figure 4. Alanine scan mutagenesis of EndoS2 active site for complex-type and high-mannose IgG1. (a) Residues on each loop predicted to make contact with either glycan were mutated individually, or in batches, to alanine, and activity was measured using mass spectrometry, normalized to wild-type EndoS2. Statistical significance compared to wild-type EndoS2 is annotated (multiple comparisons test, Tukey method; *, $p < 0.05$; **, $p < 0.01$; ***, $p < 0.001$; n.s. > 0, not significantly greater than no-enzyme control). Mutated residues are colored by loop number, with fractional activity retained compared to wild-type EndoS2 in parentheses for (b) complex-type substrate and (c) high-mannose substrate.

full-size CT glycan containing nonreducing terminal sialic acid and core fucose was used for the crystallization, electron density for only part of it could be unambiguously identified in the crystal structure (Figure 3a–c). Specifically, there was no density for the first GlcNAc, core fucose, and terminal sialic acids. The absence of the first GlcNAc and core fucose can be explained by the fact that the substrate was present with wild-type EndoS2 for days during crystallization, and the enzyme could hydrolyze the substrate between the first two GlcNAc residues, with the smaller portion diffusing away. Conversely, the terminal sialic acids are likely simply disordered in our crystal structure, as there is space to accommodate them, but no specific contacts to them. This is consistent with the observation that EndoS2 indiscriminately processes sialylated and unsialylated glycans.[3] The reducing end of the core Manβ1–4GlcNAc, the α(1,3) antenna, and α(1,6) antenna are at similar positions compared to the EndoS2-HM structure. We did not observe conformational changes between EndoS-HM and EndoS-CT crystal structures (RMSD value of 0.33 Å). Specifically, the interactions between the common core structure of CT- and HM-glycans, GlcNAc (−1), Man (−2), and Man (−7), and the residues of the loops that decorate the binding pocket are essentially conserved in EndoS2-HM and EndoS2-CT crystal structures. The main differences are that GlcNAc (−1) adopts a chair conformation, and the hydrogen bond interaction network is slightly modified between structures. In the EndoS2-CT structure, O1 of GlcNAc (−1) interacts with Q250 and E186, and the nitrogen of the acetamide group does not make contacts with D184; O4 of Man (−2) interacts with the side chain of H109, and O3 of

DOI: 10.1021/acscentsci.8b00917
ACS Cent. Sci. 2019, 5, 524–538

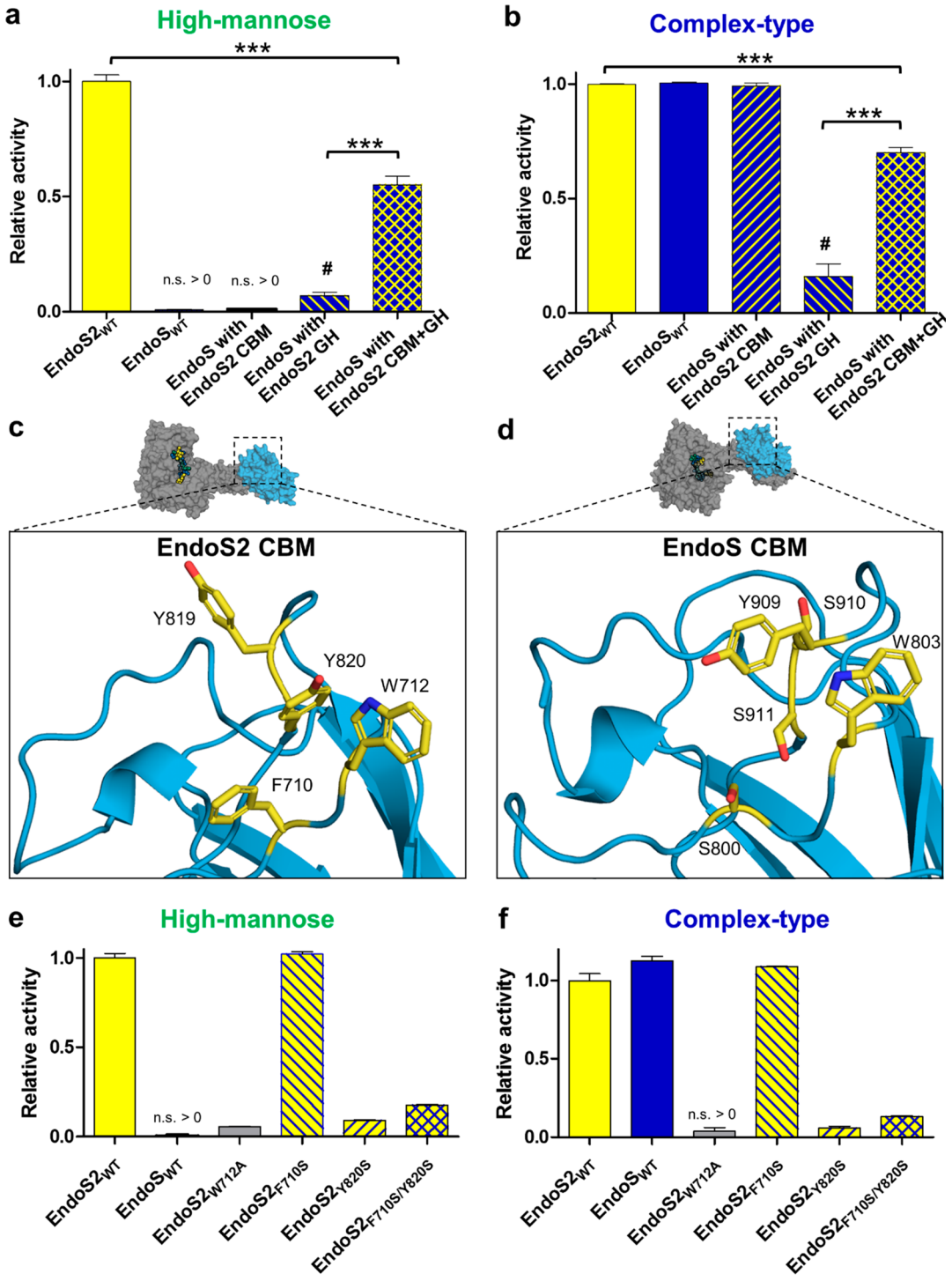

Figure 5. Hydrolytic activity of chimeric domain-swapped enzymes. (a) Hydrolytic activity of enzymes toward IgG1 bearing high-mannose *N*-glycans and (b) complex-type *N*-glycans. Activity was measured using mass spectrometry, normalized to wild-type EndoS2. Reactions were performed in technical duplicate, and error bars represent standard deviation. Statistical significance compared to wild-type EndoS2 is annotated (multiple comparisons test, Tukey method; ***, $p < 0.001$; #, $p < 0.05$ compared to no-enzyme control; n.s. > 0, not significantly greater than no-enzyme control). Comparison of glycan-binding surfaces from (c) EndoS2 and (d) EndoS (PDB 4NUZ).[19] The relative activity of specific point mutants intended to make EndoS2 more EndoS-like was tested against (e) high-mannose and (f) complex-type IgG1.

Man (−7) makes hydrogen bonds to W74 and E289 (Figure 3d and Figure S1). The α(1,6) antenna of the CT glycan binds to groove 1 of the enzyme. O6 of Man (−3), the nitrogen of the acetamide group of GlcNAc (−4), and O6 of Man (−5) interact with the side chain of D184, the main chain of D108, and the side chain of R176, respectively. The terminal sugar moieties GlcNAc (−8) and Gal (−9) do not make hydrogen bonds with the residues of the loops forming the binding pocket.

Functional Analysis of the EndoS2 Broad *N*-Glycan Specificity. Although EndoS2 forms a great number of contacts with its substrate glycans, we sought to determine

DOI: 10.1021/acscentsci.8b00917
ACS Cent. Sci. 2019, 5, 524−538

which of these contacts form the greatest contributions to binding each substrate. To investigate this, we mutated the loops that decorate the β-barrel core of the GH domain and contact the HM or CT glycans in our corresponding crystal structures. We studied the hydrolytic activity of these mutants on antibodies that bear a human IgG1 Fc and either a biantennary CT or HM *N*-glycan, and tracked reaction progression using mass spectrometry (Figure 4a). The results reveal that residues on loops 1, 6, and 7 are critical for recognition of both substrates, as mutations in these loops showed little to no activity above the no-enzyme control. In contrast, mutations in loops 2, 3, and 4 did not hinder activity for the CT *N*-glycan, and in some cases, even slightly improved it. When these results are mapped onto the crystal structure (Figure 4b), they suggest that residues which make contact with the glycan core and $\alpha(1,3)$ antenna are the major determinants of CT *N*-glycan binding for EndoS2. This binding mechanism is conserved with EndoS, which solely recognizes CT glycans, and the CT glycan structures are extremely similar in both enzymes (Figure S3). In regards to the HM substrate, mutations in loops 1, 6, and 7 also produced the greatest decreases in activity, pointing to a conserved mechanism of binding. However, mutations in loops 3 and 4 produced a moderate decrease in activity for the HM *N*-glycan, suggesting that EndoS2 fine-tunes its HM binding using these loops. Indeed, when loops 3 and 4 from EndoS are substituted into EndoS2, there is a large decrease in activity for HM, but not CT substrates. When these results are mapped onto the EndoS2-HM crystal structure (Figure 4c), it becomes apparent that EndoS2 drives binding to HM *N*-glycans using residues that make contact with the *N*-glycan core and $\alpha(1,3)$ antenna while creating space and fine-tuning binding to the $\alpha(1,6)$ antenna (Figure S3). These results are consistent with the better resolved electron density and lower B-factors for the core and $\alpha(1,3)$ antenna compared to the $\alpha(1,6)$ antenna (Figure 2c). To achieve similar reaction speeds for EndoS2 with the CT and HM substrates, we had to use ~20-fold more enzyme for the HM substrate (100 nM compared to 5 nM, with 5 μM substrate). This suggests that EndoS2 has either a slower turnover rate, or weaker binding to HM relative to CT substrates. Accordingly, we performed surface plasmon resonance binding analyses with both of these substrates, and found that catalytically dead $EndoS2_{D186L}$ binds IgG1-CT with a K_D = ~9 μM, and IgG1-HM with a K_D > 100 μM (Figure S4). EndoS binds IgG1-CT with a similar K_D (~11 μM), and does not detectably bind IgG1-HM. Taken together, these results suggest that EndoS2 has a strong preference for antibodies bearing complex-type *N*-glycans despite its ability to bind and hydrolyze high-mannose glycans on antibodies.

A search for structural homologues using the DALI server[36] revealed six endo-β-*N*-acetylglucosaminidases of the GH18 family with significant structural similarity to EndoS2 (Table S2). EndoS2 shows more structural homology with enzymes that hydrolyze CT *N*-glycans (EndoS and $EndoF_3$) than endoglycosidases that hydrolyze HM-glycans (EndoH, EndoT, EndoF1, EndoBT). Of particular relevance, EndoS2 displays 37% sequence identity with EndoS, a multidomain protein in which two additional 3-α-helical domains are attached to the N- and C-terminus (Figure S5).[18,19] EndoS, secreted by *S. pyogenes* serotype M1, specifically recognizes biantennary complex-type *N*-linked glycans of IgG Fc regions. To better understand the mechanisms of binding that differentiate EndoS2 from EndoS, we conducted a detailed analysis of the loops that decorate the corresponding active sites (Figure S1). EndoS loops 1−4, 6, and 7 all contribute contacts with the glycan, but loops 1, 6, and 7 are the main determinants of glycan binding, establishing interactions with the pentasaccharide core and $\alpha(1,3)$ antenna of the biantennary complex-type glycan.[18] These same loops have relatively high sequence conservation with EndoS2 (~50%), suggesting a conserved mechanism of glycan recognition (Figures S3 and S5). Strikingly, loops 3−5 are only ~30% conserved, and form a relatively more open space in the EndoS2 active site. This architecture provides a structural basis for EndoS2 to accommodate HM *N*-glycans, which have an additional branch on the $\alpha(1,6)$ antenna compared to biantennary CT *N*-glycans.

CBM Is Indispensable for EndoS2 To Facilitate Enzymatic Activity. The subtle but important differences between the EndoS and EndoS2 GH domain active sites led us to wonder whether these differences can fully explain the distinct specificities of the two enzymes. To test this, we created a chimeric enzyme where we swapped the EndoS2 GH domain onto an EndoS background, and tested if it would have the specificity of EndoS2 (Figure 5a,b). It did; however, its activity toward both CT and HM substrates was significantly decreased compared to wild-type EndoS2, suggesting that the GH domain is working in concert with one or more other domains to produce optimal activity. We next swapped the carbohydrate-binding module (CBM) from EndoS2 onto an EndoS background, which produced an enzyme with identical activity to wild-type EndoS. However, when we swapped both the GH and CBM domains from EndoS2 onto an EndoS background, we produced an enzyme that behaved more similarly to wild-type EndoS2. Taken together, these results suggest that the EndoS2 GH domain evolved to work with its own CBM, and that other parts of the scaffold also contribute, albeit in a less substantial way, to *N*-glycan specificity. In contrast, EndoS works equally well with either its own CBM, or the CBM from EndoS2. This led us to examine specific differences in the CBM structures that could account for their differences in supporting EndoS2 activity.

According to the DALI server, the CBM from EndoS2 most closely resembles the CBM from EndoS (PDB 4NUZ; *Z*-score = 20.6, Cα RMSD = 1.9 Å), followed by the CBM from EndoD (PDB 2XQX; *Z*-score = 16.8, Cα RMSD = 2.0 Å). Also showing high similarity are the CBMs from various chitinases (PDB 2ZY9; *Z*-score = 15.5, Cα RMSD = 2.2 Å) and sialidases (PDB 2BZD; *Z*-score = 14.8, Cα RMSD = 2.2 Å). According to the CAZy database (http://www.cazy.org/),[37] all of these proteins belong to the CBM family 32 (except EndoS, which has not been formally assigned a family). Thus, we propose that EndoS and EndoS2 both contain CBM32 domains, an assignment consistent with the description of CBM32 as a diverse and promiscuous family that is frequently appended to bacterial enzymes that interact with human *N*-glycans.[38] This family frequently binds *N*-glycans using solvent-exposed aromatic residues on loops connecting the β-sandwich scaffold.[39] Both EndoS and EndoS2 have aromatic residues in these positions, one residue of which (EndoS W803) has been reported as indispensable for substrate binding and catalysis.[19,40] At this putative *N*-glycan-binding site, EndoS2 contains two tyrosines, a tryptophan, and a phenylalanine (Figure 5c), while EndoS contains one tyrosine, three serines, and a tryptophan (Figure 5d). After confirming that the conserved tryptophan is indispensable for enzymatic activity in EndoS2 like it is in EndoS (Figure 5e,f), we sought to make

DOI: 10.1021/acscentsci.8b00917
ACS Cent. Sci. 2019, 5, 524−538

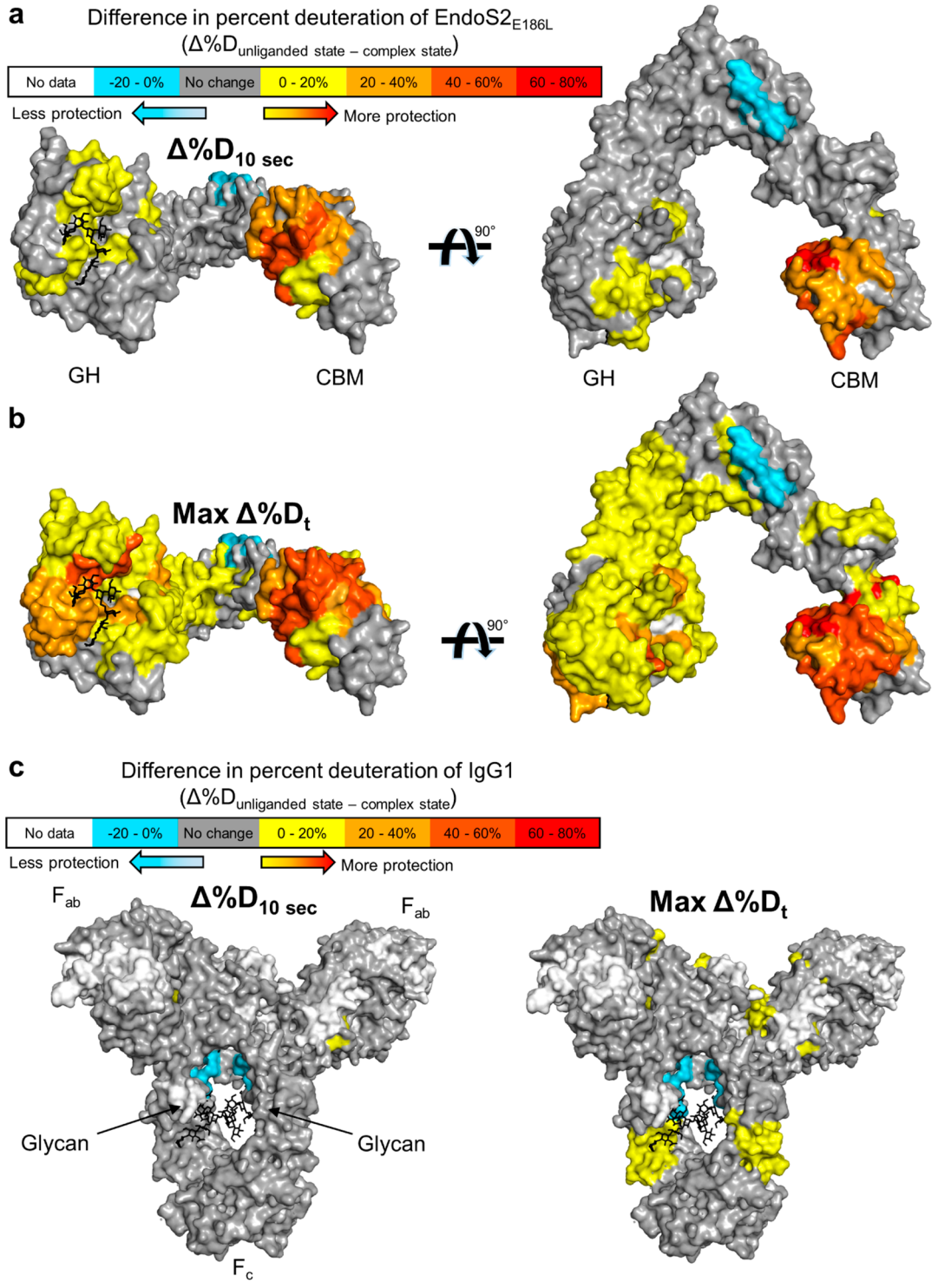

Figure 6. Hydrogen–deuterium exchange mass spectrometry. (a) Difference in deuteration between unliganded EndoS2$_{E186L}$ and IgG1-bound EndoS2$_{E186L}$ at the earliest deuterium incubation time point (10 s), mapped onto a surface representation of EndoS2. Glycoside hydrolase (GH) and carbohydrate-binding module (CBM) domains are labeled for orientation. (b) Maximum difference in deuteration of EndoS2$_{E186L}$ at any deuterium incubation time point (10 s, 1 min, 10 min, 1 h, 2 h). (c) 10 s and maximum deuteration changes between IgG1 and EndoS2$_{E186L}$-bound IgG1, mapped onto PDB 1HZH,[67] with glycosylation sites annotated.

EndoS2 more EndoS-like by selectively mutating F710 and Y820 to serine to test if this would result in a selective loss of activity toward high-mannose substrates. It did not, instead revealing that F710S has no effect on activity, while Y820S results in loss of activity toward both substrates equally. Although W712 and Y820 are both important for EndoS2 activity, these data suggest that other residues are also contributing toward the difference in the CBMs from EndoS and EndoS2.

Hydrogen–Deuterium Exchange Mass-Spectrometry (HDX-MS) Reveals the EndoS2–Antibody Interface. To gain a deeper understanding of how EndoS2 engages

DOI: 10.1021/acscentsci.8b00917
ACS Cent. Sci. 2019, 5, 524–538

antibodies using its various domains in concert, we performed HDX-MS analysis on a catalytically inactive EndoS2 variant ($EndoS2_{E186L}$) and Rituximab, both alone and in complex. HDX-MS relies on the exchange of hydrogen with deuterium on peptide backbone amides, and provides information on backbone solvent accessibility and dynamics, as residues that are more frequently exposed to solvent will undergo faster deuteration. By subtracting the percent deuteration for unliganded and complexed proteins for individual proteolytic peptides, we determined which regions of each protein display statistically significant changes in deuteration as a result of complex formation (Figure 6, Figure S6). We performed this analysis at multiple time points, as differences seen at early experimental time points (here 10 s) are often attributable to changes in protection of fast exchanging backbone amide hydrogens typically found in solvent-accessible loops (e.g., by the formation of a protein−protein or protein−carbohydrate interface), while differences that arise only at later time points can often be attributed to changes in protein dynamics of otherwise largely protected backbone amide hydrogens.[41] This analysis revealed that, at the earliest time point, large changes in protection are observed in the GH domain (specifically, loops 2, 6, and 7 where the cocrystal structure shows glycan binding) and the CBM (Figure 6a). The protection is particularly dramatic in the CBM, which includes the region that we propose to be the *N*-glycan-binding surface, as well as surrounding residues. At later time points, the protection becomes more intense in the active site and extends through the leucine-rich repeat and parts of the hybrid-Ig domain, suggesting that changes in conformational dynamics are occurring in these regions (Figure 6b). Only one region in the hybrid-Ig domain (residues 611−619) showed a loss in protection from deuterium uptake as a result of complex formation.

In stark contrast, very few changes in deuterium uptake were observed on the antibody (Figure 6c). At the earliest time point, a small decrease in protection occurs near the glycan on heavy chain residues 239−245, a pattern which has been reported to occur during antibody deglycosylation.[42] To ensure that we were not measuring antibody deglycosylation due to low residual activity in the catalytically inactive mutant, we performed mass spectrometry on the sample following HDX-MS, and found the antibody was fully glycosylated and could be deglycosylated by addition of $EndoS2_{WT}$ (Figure S7). At later time points, another region near the *N*-glycan (residues 245−264) experiences a small increase in protection, contrary to what is observed for deglycosylation.[42] It is to be noted that no data could be obtained for the *N*-glycan and three residues on either side of Asn297, a region that could be expected to make protein−protein contacts in light of their proximity to the glycan and the large HDX-MS signature induced by deglycosylation.[42] However, the large and intense protection observed in EndoS2 is not mirrored in IgG1 as they form a complex. Taken together, these data suggest that the EndoS2-IgG1 complex probed in our HDX-MS analysis forms minimal protein−protein interfaces with the antibody, instead contacting the *N*-glycans, which may become more accessible prior to deglycosylation in a pattern resembling deglycosylation. Subsequently, relatively large changes in dynamics occur on the enzyme side, while relatively small changes in dynamics occur on the antibody side.

EndoS2 might have evolved its "V-shape" with GH and CBM domains that are maintained at a particular distance apart to specifically recognize the two *N*-glycans on Asn297 of an IgG Fc. To probe the specificity of EndoS2, we created three hyperglycosylated Fc mutants that contain the wild-type Asn297 glycosylation site as well as one additional glycosylation site on a nearby solvent-exposed loop. We treated these hyperglycosylated Fc domains with EndoS2 and monitored deglycosylation by SDS-PAGE (Figure S8). The wild-type Fc is rapidly deglycosylated, but even after 1 week, the hyperglycosylated mutants only lost one pair of *N*-glycans at most, leading us to reason that only the wild-type Asn297 site was deglycosylated, as deglycosylation of the artificial site would have been followed up by rapid deglycosylation of the wild-type site. These results indicate that EndoS2 is specific for *N*-glycans located in their natural locations on IgG Fc.

EndoS2 has also been reported to deglycosylate AGP, an acute phase reactant and component of human serum, although the physiological relevance of this reaction is unclear.[3] To understand if EndoS2 uses its GH and CBM domains cooperatively to cleave AGP in a mechanism similar to IgG, we measured hydrolysis by $EndoS2_{WT}$ and CBM mutants. To detect even partial hydrolysis, we had to use very large amounts of enzyme (∼5 μM) for very long periods of time (∼48 h), results that are consistent with previously published findings[3] (Figure S9). In comparison, this is ∼1000-fold more enzyme and a ∼50-fold longer reaction time than used to completely hydrolyze IgG. Furthermore, none of the mutations in the CBM that affected IgG hydrolysis had any impact on AGP hydrolysis. Surprisingly, even $EndoS2_{E186L}$ had low but detectable activity on AGP, despite this mutant being inactive on IgG. Taken together, these results suggest that EndoS2 has $\sim 10^5$-fold reduced activity on AGP compared to IgG, with a reaction that proceeds through a different mechanism. Thus, it is possible that AGP is an incidental substrate for EndoS2.

DISCUSSION

Our data explain how EndoS2 is able to recognize a broad repertoire of *N*-glycans. Binding to substrate *N*-glycans is predominantly driven by GH domain loops 1, 6, and 7 that make contact with the *N*-glycan pentasaccharide core and $\alpha(1,3)$ antenna, a mechanism that is conserved between EndoS and EndoS2. In both enzymes, loops 6 and 7 make contact with the core alone, while loop 1 makes contact with the core and $\alpha(1,3)$ antenna; because we mutated residues in batches, we cannot be certain if binding is driven by the core alone, or the core plus $\alpha(1,3)$ antenna. Specific recognition of the $\alpha(1,3)$ antenna is plausible, as molecular dynamic simulations and NMR suggest that this antenna may be more extended and enzyme-accessible than the $\alpha(1,6)$ antenna.[43,44] EndoS2 has key differences from EndoS in GH loops 3 and 4, which create extra space and form specific contacts with the $\alpha(1,6)$ antenna (Figures 2 and 3, Figure S3). This allows EndoS2 to bind high-mannose substrates, which bear an extra antenna compared to complex biantennary substrates. This also explains how EndoS2 is able to recognize hybrid *N*-glycans, which have a complex glycan on the $\alpha(1,3)$ antenna and a high-mannose glycan on the $\alpha(1,6)$ antenna. EndoS2 also has a smaller residue than EndoS (H109 versus W153) at the position which bisects the complex glycan, which may explain why EndoS2 alone can process bisected complex *N*-glycans.[3,4] This residue interacts differently with HM- and CT-type glycan in both crystal structures. In the EndoS2-CT structure, the side chain of H109 forms a hydrogen bond with O4 of Man (−2); the

DOI: 10.1021/acscentsci.8b00917
ACS Cent. Sci. 2019, 5, 524−538

same interaction is conserved in the EndoS-CT structure mediated by W153.[18] However, in the EndoS2-HM structure, the H109 forms a hydrogen bond with the ring-oxygen of Man (−9). Even though there are no conformational changes for EndoS2 to bind HM or CT glycans, the different sugar and bond composition between glycans allows EndoS2 to accommodate either one in the binding site in a specific manner. This is not possible in other enzymes of the same family. The vast majority of contacts are made with the pentasaccharide core, which is conserved among all human *N*-glycans (Figure S1). This explains why EndoS2 does not discriminate based on the degree of sialylation, galactosylation, or fucosylation.[3] The differences in the GH domain alone are sufficient to explain the difference in specificity between EndoS and EndoS2, as demonstrated by the ability of an EndoS chimera with EndoS2 GH domain to process high-mannose IgG1 (Figure 5). However, this enzyme is extremely inefficient, but can be dramatically improved by the simultaneous substitution of the EndoS2 CBM. These results, along with CBM point mutagenesis and HDX-MS, demonstrate the critical importance of the CBM. Although EndoS2 recognizes diverse *N*-glycans, it has a strong preference for complex-type *N*-glycans on IgG. This could be due to weaker interactions within the active site (e.g., with the α[1,3] antenna), the CBM, or both. This is perhaps unsurprising from an evolutionary standpoint, as complex-type *N*-glycans make up the vast majority of glycoforms on human IgG.[45]

Our results suggest that the mechanism of EndoS2 relies on an interplay between its GH domain and CBM. Many endoglycosidases have CBMs appended to them; however, they are usually appended in seemingly random orientations relative to the GH domain, and only a few studies have investigated how the orientation of the CBM affects the activity of the GH domain.[46−50] It is tempting to speculate that the orientation of the CBM affects EndoS2 activity for several reasons. First, the GH and CBM are located on opposite tips of the "V-shaped" enzyme, with their glycan-binding surfaces pointing inward. Such a configuration could allow the CBM to bind one *N*-glycan on IgG while positioning the other near the active site. Second, when the GH and CBM domains from EndoS2 are placed on an EndoS scaffold, activity is not fully restored to wild-type levels, suggesting that the scaffold is also playing a role. Finally, EndoS2 is specific toward N297 glycosylation, as *N*-glycans that were introduced in three nearby locations were not processed. Our HDX data detect very few contacts with the antibody protein surface, so recognition is likely being driven by the *N*-glycans. The strict Asn297 specificity of EndoS2 therefore suggests something unique about the *N*-glycan structures when attached at this location as opposed to others. Perhaps the distance and angle between the GH and CBM are optimal for an avidity effect with the two *N*-glycans of intact IgG, explaining why EndoS2 loses activity on denatured IgG.[3] Structures of EndoS2 bound to Fc are tantamount to understanding the protein specificity of EndoS2, including the following: (i) what conformational changes occur in EndoS2 and IgG to support catalysis; (ii)if EndoS2 domains interact with the same *N*-glycan simultaneously, the same *N*-glycan consecutively, or two different *N*-glycans simultaneously; and (iii) if the latter is true, how the second *N*-glycan gets processed after the first is removed.

Our results also inform the field of antibody glycoengineering. In other fields, CBMs are frequently appended to carbohydrate active enzymes to increase their activity.[51−53] Our results suggest that a similar strategy could be applicable to enzymes which modify antibodies. Perhaps different CBMs could be appended to EndoS2 to shift its preference for different substrates. The same principles may also be applicable to the generation of more efficient transglycosylation mutants, which catalyze the addition rather than removal of carbohydrates. These enzymes are frequently made by mutating one of the catalytic residues in the active site, and transglycosylation mutants of EndoS2 have been described for the chemoenzymatic synthesis of IgG.[17] If transglycosylation mutants require functioning CBMs when they are naturally present, attention could be given to engineering these domains as well, and if CBMs are not required, perhaps they could be mutated or removed to slow the hydrolysis of product—a problem which frequently plagues the discovery of efficient transglycosylation mutants.

Antibodies are of considerable interest because of their versatility and central role in human health. As such, enzymes that specifically modify antibodies, such as EndoS2, may serve increasing roles in the treatment or diagnosis of disease. Understanding the mechanism of these proteins will further our ability to engineer enzymes to catalyze customizable reactions for the betterment of human health.

MATERIALS AND METHODS

Cloning, Expression, and Purification. DNA encoding wild-type EndoS2 (Genbank entry: ACI61688.1) was cloned from plasmid pGEXndoS2,[3] courtesy of Dr. M. Collin (Lund University, Sweden) into the PET22b-CPD vector as previously described.[17] The plasmid was transformed into *Escherichia coli* BL21(DE3)pLysS and expressed in 6 L of LB medium overnight at 22 °C after induction with 0.5 mM IPTG at an OD_{600} of 0.6. Cells were harvested (5000*g* for 15 min) and lysed in a buffer containing 500 mM NaCl, 10% (v/v) glycerol, and 50 mM Tris-HCl pH 7.4 (buffer 1) by sonication. The soluble fraction was passed over a HisPur NiNTA column (Thermo Scientific), and washed with buffer 1 until absorbance at 280 nm was undetectable. EndoS2 was then eluted using buffer 1 supplemented with 100 μM phytic acid for 10 min at room temperature to remove the CPD-His_{10} domain.[54] EndoS2 was concentrated in an Amicon Ultra-15 centrifugal filter unit (Millipore) with a molecular cutoff of 50 kDa at 4000*g*, and exchanged into a buffer containing 75 mM NaCl, 10 mM Tris-HCl pH 7.4 (buffer 2) for crystallization studies, or PBS for enzymatic studies. EndoS2 was then further purified by size exclusion chromatography in a Superdex 200 10/300 GL column (GE Healthcare), and assessed for purity by SDS/PAGE. EndoS2 alanine mutants were developed by PCR-based site-directed mutagenesis, while loop-swap and domain-swap chimeras were created by the FastCloning method,[55] with full sequences confirmed by Stabvida (https://www.stabvida.com) or Genewiz (https://www.genewiz.com) (Table S3). The template for *ndoS* came from pGEXndoS (GenBank entry: AF296340).[19] EndoS2 mutants were expressed and purified as described above, flash-frozen, and stored at −20 °C until ready for use.

Chemoenzymatic Preparation of *N*-Glycans. The core fucosylated sialyl complex-type *N*-glycan (G2S2F) was synthesized through enzymatic core fucosylation of the sialylated glycopeptide (SGP) isolated from chicken egg yolks, followed by PNGase F catalyzed release of the free *N*-glycan from the glycopeptide. Specifically, the α-fucoligase mutant E274A (0.28 mg, 0.28 mg/mL) was added to a mixture

DOI: 10.1021/acscentsci.8b00917
ACS Cent. Sci. 2019, 5, 524−538

of α-fucopyranosyl fluoride (0.5 mg, 3 μmol) and acceptor SGP (5.72 mg, 2 μmol) in a buffer (PBS, 100 mM, pH 7.4, 1 mL).[56] The reaction was monitored with LC-MS (Thermo Scientific), and the desired product was purified with preparative HPLC (Waters) to give the fucosylated glycopeptide, G2S2F-peptide (5.16 mg, 86%). ESI-MS: calcd for SGP-F, M = 3011.23 Da; found (*m*/*z*), 1507.32 $[M + 2H]^{2+}$, 1005.41 $[M + 3H]^{3+}$. A solution of the G2S2F-peptide (5 mg) in a buffer (PBS, 100 mM, pH 7.4, 0.5 mL) was incubated with PNGase F (100 μg at 37 °C for 2 h. The desired product was purified with G-10 size-exclusion column (GE Healthcare) to give the core fucosylated *N*-glycan, G2S2F (3.1 mg, 80%). ESI-MS: calcd for SCT-F, M = 2368.84 Da; found (*m*/*z*), 1186.10 $[M + 2H]^{2+}$, 790.89 $[M + 3H]^{3+}$. The high-mannose (HM, $Man_9GlcNAc_2Asn$) glycan was prepared by digestion of soybean agglutinin isolated from soybean flour, following the previously published procedure.[57] ESI-MS: calcd for Man9-GlcNAc2Asn, M = 1996.69 Da; found (*m*/*z*), 999.99 $[M + 2H]^{2+}$, 680.13 $[M + 3Na]^{3+}$.

EndoS2 Crystallization and Data Collection. Wild-type EndoS2 was concentrated to 7 mg/mL, and 250 nL of protein was combined with 250 nL of mother liquor (0.2 M sodium citrate tribasic, 0.1 M sodium citrate pH 4, and 20% [w/v] polyethylene glycol 3350) in sitting drops. Crystals resembling a hair ball were discovered six months later, having previously been checked after one month. Crystal morphology was improved by streak seeding into hanging drops where 1 μL of protein at 6.6 mg/mL was combined with 1 μL of mother liquor, resulting in the appearance of single platelike crystals after 3 days. These unliganded crystals were harvested in mother liquor supplemented with 20% (v/v) glycerol for cryoprotection, and flash cooled in liquid nitrogen. EndoS2-CT crystals were obtained by cocrystallizing EndoS2, as described above, with mother liquor supplemented with 2 mM CT glycan, and then harvested into mother liquor supplemented with 20% glycerol and 1.1 mM CT glycan and flash cooled. EndoS2-HM crystals were obtained by soaking unliganded crystals in mother liquor supplemented with 50 mM Man_9 *N*-glycan and 20% glycerol for 1 min before being flash cooled. Data were collected from unliganded EndoS2 and EndoS2-CT crystals at the Stanford Synchrotron Radiation Lightsource (SSRL) beamline 12-2 using a Dectris Pilatus3 6 M detector. Data for EndoS2-HM were collected at the Advanced Photon Source (APS) beamline 23-ID-D on a Dectris Pilatus3 6 M detector.

Structure Determination, Refinement, and Analysis. The unliganded EndoS2 structure was solved first, using the GH, LRR, and hybrid-Ig domains from EndoS as a search model for molecular replacement using PHENIX Phaser-MR.[58] Subsequent rounds of model building and refinement using Coot[59] and phenix.refine,[60] respectively, allowed for molecular replacement of the remaining CBM domain. Models were further built and refined, and then run through the PDB_REDO server[61] before a final round of refinement with phenix.refine. EndoS2-CT and EndoS2-HM were phased off of the unliganded EndoS2 structure, and then built and refined as described above. The glycans were built using the GLYCAM−Web server (http://glycam.org/) and energy-minimized using the PRODRG server,[62] and restraints were generated using the grade web server (http://grade.globalphasing.org). *Z*-scores were produced using DALI.[36] Protein−ligand contacts were determined using the PISA server[63] and further refined using the following distance cutoffs (in Å): C−C, 4.1; C−N, 3.8; C−O, 3.7; O−O, 3.3; O−N, 3.4; N−N, 3.4.[64] Illustrations were generated using PyMOL2.2 (Schrödinger, 2018).

Production of Antibodies. Rituximab (RITUXAN, Genentech) was kindly provided courtesy of the University of Maryland Greenebaum Comprehensive Cancer Center. High-mannose IgG1 antibodies were expressed and purified from HEK293T cells as previously described.[18] Hyperglycosylated Fcs (IgG1 C_H residues 238−447) were generated through point mutagenesis by introducing the glycosylation motif NST into various surface-exposed loops near the natural glycosylation site. These Fcs contained the natural glycosylation site at N297, as well as an additional glycosylation site at either N267, N325, or N329. Wild-type and hyperglycosylated Fcs were cloned into pcDNA4/to, and then transfected using polyethylenimine as transfection reagent. After transfection, cells were cultured for 96 h in Free-style F17 medium supplemented with GlutaMAX and Geneticin (Thermo FisherScientific). Hyperglycosylated Fcs were purified from culture supernatants by protein A chromatography using 20 mM sodium phosphate buffer pH 7.0 as binding buffer and 100 mM sodium citrate buffer pH 3.0 as elution buffer. All the fractions were neutralized with 1 M Tris pH 9.0, pooled and dialyzed against 20 mm HEPES pH 7.4, 150 mM NaCl, and further purified by size exclusion chromatography in a Superdex 200 10/300 GL column (GE Healthcare). The presence of hyperglycosylation was confirmed by SDS-PAGE.

Enzymatic Activity Assays. Reactions were set up using 5 nM EndoS2 for reactions with Rituximab, or 100 nM EndoS2 for reactions with high-mannose IgG1. Enzymes were mixed with 5 μM antibody in PBS pH 7.4 at room temperature. For point mutants, 10 μL aliquots of the reaction were taken in duplicate and quenched after 45 min with 1.1 μL of 1% trifluoroacetic acid. Longer reaction times were used to detect lower levels of activity; domain-swap reactions were allowed to progress for 2 h, and hyperglycosylation reactions were allowed to progress for 6 days. The quenched reactions were then mixed with 50 mM TCEP, and analyzed by LC-MS using an Accela LC System attached to a LXQ linear ion trap mass spectrometer (Thermo Scientific, Waltham, MA), as previously described.[65] Relative amounts of substrate and hydrolysis products were quantified after deconvolution of the raw data and identification of the corresponding MS peaks using BioWorks (Thermo Scientific, Waltham, MA). Statistical significance was determined using a multiple comparisons test (Tukey method) in GraphPad (GraphPad Software, La Jolla, CA). No difference in activity was observed for EndoS2 before and after flash-freezing. For α-1-AGP hydrolysis, lyophilized α-1-AGP (Sigma) was resuspended in PBS, and 8 μg of α-1-AGP was added to 4 μg of enzyme in 20 μL of PBS, and incubated at 37 °C for up to 48 h. Reactions were quenched by boiling in Laemmli buffer, and results were analyzed by SDS-PAGE.

Binding Analysis. Surface plasmon resonance experiments were performed as previously described,[19] with the following modifications: Rituximab was immobilized in flow cells 1 and 2, while high-mannose IgG1 was immobilized in flow cells 3 and 4—both at a density of 1000 RU. *N*-Glycans were removed from flow cells 1 and 3 by flowing 1 mg/mL $EndoS2_{WT}$ over these cells for 1 h. The HBS-X running buffer contained 20 mM HEPES pH 7.4, 150 mM NaCl, and 0.005% Tween 20. Concentration series of $EndoS2_{E186L}$ (20−0.32 μM) and $EndoS_{E235L}$ (20−0.32 μM) were injected over flow cells 1

DOI: 10.1021/acscentsci.8b00917
ACS Cent. Sci. 2019, 5, 524−538

and 2 to measure Rituximab binding, while concentration series of EndoS2$_{E186L}$ (100−0.78 μM) and EndoS$_{E235L}$ (80−0.63 μM) were injected over flow cells 3 and 4 to measure high-mannose IgG1 binding.

Hydrogen−Deuterium Exchange Mass Spectrometry (HDX-MS). The coverage maps for all proteins were obtained from undeuterated controls as follows: 1 μL of 200 μM sample in PBS was diluted with 19 μL of ice cold quench (50 mM glycine, 6.8 M guanidine-HCl, 100 mM tris(2-carboxyethyl)-phosphine [TCEP], pH 2.4). After 5 min, 180 μL of 50 mM glycine buffer, pH 2.4, was added prior to the injection. A 50 μL portion of quenched samples was injected into a Waters HDX nanoAcquity UPLC (Waters, Milford, MA) with in-line pepsin digestion (Waters Enzymate BEH pepsin column). Peptic fragments were trapped on an Acquity UPLC BEH C18 peptide trap and separated on an Acquity UPLC BEH C18 column. A 7 min, 5−35% acetonitrile (0.1% formic acid) gradient was used to elute peptides directly into a Waters Synapt G2-Si mass spectrometer (Waters, Milford, MA). MSE data were acquired with a 20−30 V ramp trap CE for high-energy acquisition of product ions as well as continuous lock mass (Leu-Enk) for mass accuracy correction. Peptides were identified using the ProteinLynx Global server 3.0.3 (PLGS) from Waters. Further filtering of 0.3 fragments per residue was applied in DynamX 3.0.

For each construct, the HD exchange reactions and controls were acquired using a LEAP autosampler controlled by Chronos software. The reactions were performed as follows: 1 μL of 100 μM unliganded EndoS2$_{E186L}$, unliganded Rituximab, or EndoS2$_{E186L}$ in complex with Rituximab in PBS was incubated in 19 μL of PBS, 99.99% D_2O, pD 7.4. All reactions were performed at 25 °C. Prior to injection, deuteration reactions were quenched at various times (10 s, 1 min, 10 min, 1 h, and 2 h) with 60 μL of 50 mM glycine buffer, 7 M guanidine-HCl, 100 mM TCEP pH 2.4, followed 1 min later by a postquench dilution of 170 μL of 50 mM glycine buffer, pH 2.4. A volume of 55 μL of the quenched reaction was injected. Back exchange correction was performed against fully deuterated controls acquired by incubating 1 μL of 100 μM of each sample in 19 μL of PBS, 99.99% D_2O, pD 7.4 containing 7 M deuterated guanidine DCl and 30 mM TCEP for 2 h at 25 °C prior to quenching (without guanidine HCl) and dilution. All deuteration time points and controls were acquired in triplicate.

The deuterium uptake for all identified peptides with increasing deuteration time and for the fully deuterated control was determined using Water's DynamX 3.0 software. The normalized percentage of deuterium uptake at an incubation time t ($\%D_t$) for a given peptide was calculated as follows: $\%D_t = \frac{100(m_t - m_0)}{m_f - m_0}$, with m_t the centroid mass at incubation time t, m_0 the centroid mass of the undeuterated control, and m_f the centroid mass of the fully deuterated control. Percent deuteration difference plots, $\Delta\%D_t$ (unliganded − complex), displaying the difference in percent deuteration between the unliganded and Rituximab-complexed EndoS2$_{E186L}$ for all identified peptides, at all deuterium incubation times probed were generated. Confidence intervals for the $\Delta\%D$ plots were determined using the method outlined by Houde et al.,[66] adjusted to percent deuteration using the fully deuterated controls. Briefly, this approach involves the use of a two-criteria condition for determining the statistical significance of deuterium uptake differences observed for any given peptide: first, a difference in deuterium uptake at any single deuterium incubation time point (in colors) which is superior to the 98% confidence interval (thin horizontal lines) as determined using the overall standard deviation from the entire data set (all peptides, all time points, all states); and second, a summed difference in deuterium uptake integrated over all time points probed (represented as gray bars) which is superior to its respective 98% confidence interval (thick horizontal lines) as determined using the overall standard deviation propagated to the number of time point.

■ ASSOCIATED CONTENT

Supporting Information

The Supporting Information is available free of charge on the ACS Publications website at DOI: 10.1021/acscentsci.8b00917.

Crystallography statistics, table of related enzymes, summary of enzyme constructs, diagram of enzyme/substrate contacts, details on GlcNAc −1 "skew-boat" conformation, structural comparison of EndoS/EndoS2 active sites, surface plasmon resonance analysis, sequence alignment of EndoS/EndoS2 active sites, HDX-MS details, mass spectrometry controls, hydrolysis of hyperglycosylated Fc, and hydrolysis of α-1-AGP (PDF)

Accession Codes

The atomic coordinates have been deposited in the Protein Data Bank, www.pdb.org (PDB ID codes 6E58 [unliganded], 6MDV [high-mannose], and 6MDS [complex-type]).

■ AUTHOR INFORMATION

Corresponding Authors

*E-mail: mrcguerin@cicbiogune.es.
*E-mail: ESundberg@som.umaryland.edu.

ORCID

Erik H. Klontz: 0000-0002-1923-972X
Daniel Deredge: 0000-0002-6897-6523
Chao Li: 0000-0002-8090-2017
Lai-Xi Wang: 0000-0003-4293-5819
Marcelo E. Guerin: 0000-0001-9524-3184
Eric J. Sundberg: 0000-0003-0478-3033

Author Contributions

¶E.H.K. and B.T. contributed equally to this work. E.J.S., L.-X.W., and M.E.G. conceived the project. E.H.K., B.T., C.L., J.O., D.D., J.K.F., and J.F. performed the experiments. E.H.K., B.T., D.D., S.G., J.K.F., P.L.W., E.J.S., and M.E.G. analyzed the results. E.H.K., B.T., E.J.S., and M.E.G. wrote the manuscript.

Notes

Safety statement: no unexpected or unusually high safety hazards were encountered.
The authors declare no competing financial interest.

■ ACKNOWLEDGMENTS

This research used resources of the Advanced Photon Source, a U.S. Department of Energy (DOE) Office of Science User Facility operated for the DOE Office of Science by Argonne National Laboratory under Contract DE-AC02-06CH11357. Additionally, use of the Stanford Synchrotron Radiation Lightsource, SLAC National Accelerator Laboratory, is supported by the U.S. Department of Energy, Office of Science, Office of Basic Energy Sciences under Contract DE-

DOI: 10.1021/acscentsci.8b00917
ACS Cent. Sci. 2019, 5, 524−538

AC02-76SF00515. The SSRL Structural Molecular Biology Program is supported by the DOE Office of Biological and Environmental Research, and by the National Institutes of Health, National Institute of General Medical Sciences (including P41GM103393). This work is also supported in part by the University of Maryland Baltimore, School of Pharmacy Mass Spectrometry Center (SOP1841-IQB2014), MINECO/FEDER EU Contracts BFU2016-7427-C2-2-R, Severo Ochoa Excellence Accreditation SEV-2016-0644 (M.E.G.), MINECO/FEDER EU under the "Juan de la Cierva Postdoctoral program", Contract IJCI-2014-19206 (B.T.), as well as NIH T32 AI095190 (E.H.K.), and NIH R01 GM096973 (L.-X.W.). The funders had no role in study design, data collection and interpretation, or the decision to submit the work for publication. The content is solely the responsibility of the authors and does not necessarily represent the official views of the National Institutes of Health.

REFERENCES

(1) Cymer, F.; Beck, H.; Rohde, A.; Reusch, D. Therapeutic monoclonal antibody N-glycosylation - Structure, function and therapeutic potential. *Biologicals* **2018**, *52*, 1−11.

(2) Collin, M.; Olsen, A. EndoS, a novel secreted protein from *Streptococcus pyogenes* with endoglycosidase activity on human IgG. *EMBO J.* **2001**, *20* (12), 3046−3055.

(3) Sjogren, J.; Struwe, W. B.; Cosgrave, E. F.; Rudd, P. M.; Stervander, M.; Allhorn, M.; Hollands, A.; Nizet, V.; Collin, M. EndoS2 is a unique and conserved enzyme of serotype M49 group A *Streptococcus* that hydrolyses N-linked glycans on IgG and alpha1-acid glycoprotein. *Biochem. J.* **2013**, *455* (1), 107−118.

(4) Goodfellow, J. J.; Baruah, K.; Yamamoto, K.; Bonomelli, C.; Krishna, B.; Harvey, D. J.; Crispin, M.; Scanlan, C. N.; Davis, B. G. An endoglycosidase with alternative glycan specificity allows broadened glycoprotein remodelling. *J. Am. Chem. Soc.* **2012**, *134* (19), 8030−8033.

(5) Nandakumar, K. S.; Collin, M.; Happonen, K. E.; Lundstrom, S. L.; Croxford, A. M.; Xu, B.; Zubarev, R. A.; Rowley, M. J.; Blom, A. M.; Kjellman, C.; et al. *Streptococcal* endo-beta-N-acetylglucosaminidase suppresses antibody-mediated inflammation in vivo. *Front. Immunol.* **2018**, *9*, 1623.

(6) Mihai, S.; Albert, H.; Ludwig, R. J.; Iwata, H.; Bjorck, L.; Collin, M.; Nimmerjahn, F. In vivo enzymatic modulation of IgG antibodies prevents immune complex-dependent skin injury. *Exp Dermatol* **2017**, *26* (8), 691−696.

(7) Lood, C.; Allhorn, M.; Lood, R.; Gullstrand, B.; Olin, A. I.; Ronnblom, L.; Truedsson, L.; Collin, M.; Bengtsson, A. A. IgG glycan hydrolysis by endoglycosidase S diminishes the proinflammatory properties of immune complexes from patients with systemic lupus erythematosus: a possible new treatment? *Arthritis Rheum.* **2012**, *64* (8), 2698−2706.

(8) Collin, M.; Shannon, O.; Bjorck, L. IgG glycan hydrolysis by a bacterial enzyme as a therapy against autoimmune conditions. *Proc. Natl. Acad. Sci. U. S. A.* **2008**, *105* (11), 4265−4270.

(9) Baruah, K.; Bowden, T. A.; Krishna, B. A.; Dwek, R. A.; Crispin, M.; Scanlan, C. N. Selective deactivation of serum IgG: a general strategy for the enhancement of monoclonal antibody receptor interactions. *J. Mol. Biol.* **2012**, *420* (1−2), 1−7.

(10) Iwamoto, M.; Yamaguchi, T.; Sekiguchi, Y.; Oishi, S.; Shiiki, T.; Soma, M.; Nakamura, K.; Yoshida, M.; Chaya, H.; Mori, Y.; et al. Pharmacokinetic and pharmacodynamic profiles of glyco-modified atrial natriuretic peptide derivatives synthesized using chemo-enzymatic synthesis approaches. *Bioconjugate Chem.* **2018**, *29* (8), 2829−2837.

(11) Huang, W.; Giddens, J.; Fan, S. Q.; Toonstra, C.; Wang, L. X. Chemoenzymatic glycoengineering of intact IgG antibodies for gain of functions. *J. Am. Chem. Soc.* **2012**, *134* (29), 12308−12318.

(12) Li, C.; Wang, L. X. Chemoenzymatic methods for the synthesis of glycoproteins. *Chem. Rev.* **2018**, *118* (17), 8359−8413.

(13) Vanderschaeghe, D.; Meuris, L.; Raes, T.; Grootaert, H.; Van Hecke, A.; Verhelst, X.; Van de Velde, F.; Lapauw, B.; Van Vlierberghe, H.; Callewaert, N. Endoglycosidase S enables a highly simplified clinical chemistry assay procedure for direct assessment of serum IgG undergalactosylation in chronic inflammatory disease. *Mol. Cell. Proteomics* **2018**, *17*, 2508.

(14) Jordan, S. C.; Lorant, T.; Choi, J.; Kjellman, C.; Winstedt, L.; Bengtsson, M.; Zhang, X.; Eich, T.; Toyoda, M.; Eriksson, B. M.; et al. IgG Endopeptidase in Highly Sensitized Patients Undergoing Transplantation. *N. Engl. J. Med.* **2017**, *377* (5), 442−453.

(15) Sha, S.; Agarabi, C.; Brorson, K.; Lee, D. Y.; Yoon, S. N-glycosylation design and control of therapeutic monoclonal antibodies. *Trends Biotechnol.* **2016**, *34* (10), 835−846.

(16) Sjogren, J.; Collin, M. Bacterial glycosidases in pathogenesis and glycoengineering. *Future Microbiol.* **2014**, *9* (9), 1039−1051.

(17) Li, T.; Tong, X.; Yang, Q.; Giddens, J. P.; Wang, L. X. Glycosynthase mutants of Endoglycosidase S2 show potent transglycosylation activity and remarkably relaxed substrate specificity for antibody glycosylation remodeling. *J. Biol. Chem.* **2016**, *291* (32), 16508−16518.

(18) Trastoy, B.; Klontz, E.; Orwenyo, J.; Marina, A.; Wang, L. X.; Sundberg, E. J.; Guerin, M. E. Structural basis for the recognition of complex-type N-glycans by Endoglycosidase S. *Nat. Commun.* **2018**, *9* (1), 1874.

(19) Trastoy, B.; Lomino, J. V.; Pierce, B. G.; Carter, L. G.; Gunther, S.; Giddens, J. P.; Snyder, G. A.; Weiss, T. M.; Weng, Z.; Wang, L. X.; et al. Crystal structure of *Streptococcus pyogenes* EndoS, an immunomodulatory endoglycosidase specific for human IgG antibodies. *Proc. Natl. Acad. Sci. U. S. A.* **2014**, *111* (18), 6714−6719.

(20) Dixon, E. V.; Claridge, J. K.; Harvey, D. J.; Baruah, K.; Yu, X.; Vesiljevic, S.; Mattick, S.; Pritchard, L. K.; Krishna, B.; Scanlan, C. N.; et al. Fragments of bacterial endoglycosidase s and immunoglobulin g reveal subdomains of each that contribute to deglycosylation. *J. Biol. Chem.* **2014**, *289* (20), 13876−13889.

(21) Boraston, A. B.; Bolam, D. N.; Gilbert, H. J.; Davies, G. J. Carbohydrate-binding modules: fine-tuning polysaccharide recognition. *Biochem. J.* **2004**, *382* (3), 769−781.

(22) Henrissat, B.; Davies, G. Structural and sequence-based classification of glycoside hydrolases. *Curr. Opin. Struct. Biol.* **1997**, *7* (5), 637−644.

(23) Davies, G.; Henrissat, B. Structures and mechanisms of glycosyl hydrolases. *Structure* **1995**, *3* (9), 853−859.

(24) Jitonnom, J.; Lee, V. S.; Nimmanpipug, P.; Rowlands, H. A.; Mulholland, A. J. Quantum mechanics/molecular mechanics modeling of substrate-assisted catalysis in family 18 chitinases: conformational changes and the role of Asp142 in catalysis in ChiB. *Biochemistry* **2011**, *50* (21), 4697−4711.

(25) van Aalten, D. M.; Komander, D.; Synstad, B.; Gaseidnes, S.; Peter, M. G.; Eijsink, V. G. Structural insights into the catalytic mechanism of a family 18 exo-Chitinase. *Proc. Natl. Acad. Sci. U. S. A.* **2001**, *98* (16), 8979−8984.

(26) White, A.; Rose, D. R. Mechanism of catalysis by retaining beta-glycosyl hydrolases. *Curr. Opin. Struct. Biol.* **1997**, *7* (5), 645−651.

(27) Williams, S. J.; Mark, B. L.; Vocadlo, D. J.; James, M. N.; Withers, S. G. Aspartate 313 in the *Streptomyces plicatus* hexosaminidase plays a critical role in substrate-assisted catalysis by orienting the 2-acetamido group and stabilizing the transition state. *J. Biol. Chem.* **2002**, *277* (42), 40055−40065.

(28) Chen, L.; Liu, T.; Zhou, Y.; Chen, Q.; Shen, X.; Yang, Q. Structural characteristics of an insect group I Chitinase, an enzyme indispensable to moulting. *Acta Crystallogr., Sect. D: Biol. Crystallogr.* **2014**, *70* (4), 932−942.

(29) Fadel, F.; Zhao, Y.; Cachau, R.; Cousido-Siah, A.; Ruiz, F. X.; Harlos, K.; Howard, E.; Mitschler, A.; Podjarny, A. New insights into the enzymatic mechanism of human chitotriosidase (CHIT1) catalytic domain by atomic resolution X-ray diffraction and hybrid

DOI: 10.1021/acscentsci.8b00917
ACS Cent. Sci. 2019, 5, 524−538

QM/MM. *Acta Crystallogr., Sect. D: Biol. Crystallogr.* **2015**, *71* (7), 1455−1470.
(30) Hsieh, Y. C.; Wu, Y. J.; Chiang, T. Y.; Kuo, C. Y.; Shrestha, K. L.; Chao, C. F.; Huang, Y. C.; Chuankhayan, P.; Wu, W. G.; Li, Y. K.; et al. Crystal structures of *Bacillus cereus NCTU2* Chitinase complexes with chitooligomers reveal novel substrate binding for catalysis: a Chitinase without chitin binding and insertion domains. *J. Biol. Chem.* **2010**, *285* (41), 31603−31615.
(31) Itoh, T.; Hibi, T.; Suzuki, F.; Sugimoto, I.; Fujiwara, A.; Inaka, K.; Tanaka, H.; Ohta, K.; Fujii, Y.; Taketo, A.; et al. Crystal structure of Chitinase ChiW from *Paenibacillus sp. str. FPU-7* reveals a novel type of bacterial cell-surface-expressed multi-modular enzyme machinery. *PLoS One* **2016**, *11* (12), No. e0167310.
(32) Malecki, P. H.; Raczynska, J. E.; Vorgias, C. E.; Rypniewski, W. Structure of a complete four-domain Chitinase from Moritella marina, a marine psychrophilic bacterium. *Acta Crystallogr., Sect. D: Biol. Crystallogr.* **2013**, *69* (5), 821−829.
(33) Ranok, A.; Wongsantichon, J.; Robinson, R. C.; Suginta, W. Structural and thermodynamic insights into chitooligosaccharide binding to human cartilage Chitinase 3-like protein 2 (CHI3L2 or YKL-39). *J. Biol. Chem.* **2015**, *290* (5), 2617−2629.
(34) Coines, J.; Alfonso-Prieto, M.; Biarnes, X.; Planas, A.; Rovira, C. Oxazoline or oxazolinium ion? The protonation state andc conformation of the reaction intermediate of Chitinase enzymes revisited. *Chem. - Eur. J.* **2018**, *24* (72), 19258−19265.
(35) Speciale, G.; Thompson, A. J.; Davies, G. J.; Williams, S. J. Dissecting conformational contributions to glycosidase catalysis and inhibition. *Curr. Opin. Struct. Biol.* **2014**, *28*, 1−13.
(36) Holm, L.; Rosenstrom, P. Dali server: conservation mapping in 3D. *Nucleic Acids Res.* **2010**, *38* (s2), W545−W549.
(37) Lombard, V.; Golaconda Ramulu, H.; Drula, E.; Coutinho, P. M.; Henrissat, B. The carbohydrate-active enzymes database (CAZy) in 2013. *Nucleic Acids Res.* **2014**, *42* (D1), D490−D495.
(38) Abbott, D. W.; Eirin-Lopez, J. M.; Boraston, A. B. Insight into ligand diversity and novel biological roles for family 32 carbohydrate-binding modules. *Mol. Biol. Evol.* **2007**, *25* (1), 155−167.
(39) Abbott, D. W.; Boraston, A. Structural analysis of a putative family 32 carbohydrate-binding module from the *Streptococcus pneumoniae* enzyme EndoD. *Acta Crystallogr., Sect. F: Struct. Biol. Cryst. Commun.* **2011**, *67* (4), 429−433.
(40) Allhorn, M.; Olsen, A.; Collin, M. EndoS from *Streptococcus pyogenes* is hydrolyzed by the cysteine proteinase SpeB and requires glutamic acid 235 and tryptophans for IgG glycan-hydrolyzing activity. *BMC Microbiol.* **2008**, *8*, 3.
(41) Morgan, C. R.; Engen, J. R. Investigating solution-phase protein structure and dynamics by hydrogen exchange mass spectrometry. *Curr. Protoc Protein Sci.* **2009**, 17-6-1−17-6-17.
(42) Houde, D.; Arndt, J.; Domeier, W.; Berkowitz, S.; Engen, J. R. Characterization of IgG1 conformation and conformational dynamics by hydrogen/deuterium exchange mass spectrometry. *Anal. Chem.* **2009**, *81* (14), 2644−2651.
(43) Harbison, A. M.; Brosnan, L. P.; Fenlon, K.; Fadda, E. Sequence to structure dependence of isolated IgG Fc complex biantennary N-glycans: A molecular dynamics study. *Glycobiology* **2019**, *29* (1), 94−103.
(44) Barb, A. W.; Prestegard, J. H. NMR analysis demonstrates immunoglobulin G N-glycans are accessible and dynamic. *Nat. Chem. Biol.* **2011**, *7* (3), 147−153.
(45) Pucic, M.; Knezevic, A.; Vidic, J.; Adamczyk, B.; Novokmet, M.; Polasek, O.; Gornik, O.; Supraha-Goreta, S.; Wormald, M. R.; Redzic, I.; et al. High throughput isolation and glycosylation analysis of IgG-variability and heritability of the IgG glycome in three isolated human populations. *Mol. Cell. Proteomics* **2011**, *10* (10), M111.010090.
(46) Tajwar, R.; Shahid, S.; Zafar, R.; Akhtar, M. W. Impact of orientation of carbohydrate binding modules family 22 and 6 on the catalytic activity of *Thermotoga maritima* xylanase XynB. *Enzyme Microb. Technol.* **2017**, *106*, 75−82.
(47) Correia, M. A.; Mazumder, K.; Bras, J. L.; Firbank, S. J.; Zhu, Y.; Lewis, R. J.; York, W. S.; Fontes, C. M.; Gilbert, H. J. Structure and function of an arabinoxylan-specific xylanase. *J. Biol. Chem.* **2011**, *286* (25), 22510−22520.
(48) Cuskin, F.; Flint, J. E.; Gloster, T. M.; Morland, C.; Basle, A.; Henrissat, B.; Coutinho, P. M.; Strazzulli, A.; Solovyova, A. S.; Davies, G. J.; et al. How nature can exploit nonspecific catalytic and carbohydrate binding modules to create enzymatic specificity. *Proc. Natl. Acad. Sci. U. S. A.* **2012**, *109* (51), 20889−20894.
(49) Lammerts van Bueren, A.; Ficko-Blean, E.; Pluvinage, B.; Hehemann, J. H.; Higgins, M. A.; Deng, L.; Ogunniyi, A. D.; Stroeher, U. H.; El Warry, N.; Burke, R. D.; et al. The conformation and function of a multimodular glycogen-degrading pneumococcal virulence factor. *Structure* **2011**, *19* (5), 640−651.
(50) Abbott, D. W.; van Bueren, A. L. Using structure to inform carbohydrate binding module function. *Curr. Opin. Struct. Biol.* **2014**, *28*, 32−40.
(51) Arumugam Mahadevan, S.; Wi, S. G.; Lee, D. S.; Bae, H. J. Site-directed mutagenesis and CBM engineering of Cel5A (*Thermotoga maritima*). *FEMS Microbiol. Lett.* **2008**, *287* (2), 205−211.
(52) Mamo, G.; Hatti-Kaul, R.; Mattiasson, B. Fusion of carbohydrate binding modules from *Thermotoga neapolitana* with a family 10 xylanase from *Bacillus halodurans* S7. *Extremophiles* **2007**, *11* (1), 169−177.
(53) Zhang, J.; Moilanen, U.; Tang, M.; Viikari, L. The carbohydrate-binding module of xylanase from *Nonomuraea flexuosa* decreases its non-productive adsorption on lignin. *Biotechnol. Biofuels* **2013**, *6* (1), 18.
(54) Shen, A.; Lupardus, P. J.; Morell, M.; Ponder, E. L.; Sadaghiani, A. M.; Garcia, K. C.; Bogyo, M. Simplified, enhanced protein purification using an inducible, autoprocessing enzyme tag. *PLoS One* **2009**, *4* (12), No. e8119.
(55) Li, C.; Wen, A.; Shen, B.; Lu, J.; Huang, Y.; Chang, Y. FastCloning: a highly simplified, purification-free, sequence- and ligation-independent PCR cloning method. *BMC Biotechnol.* **2011**, *11*, 92.
(56) Li, C.; Zhu, S.; Ma, C.; Wang, L. X. Designer alpha1,6-fucosidase mutants enable direct core fucosylation of intact N-glycopeptides and N-glycoproteins. *J. Am. Chem. Soc.* **2017**, *139* (42), 15074−15087.
(57) Wang, L. X.; Ni, J.; Singh, S.; Li, H. Binding of high-mannose-type oligosaccharides and synthetic oligomannose clusters to human antibody 2G12: implications for HIV-1 vaccine design. *Chem. Biol.* **2004**, *11* (1), 127−134.
(58) McCoy, A. J.; Grosse-Kunstleve, R. W.; Adams, P. D.; Winn, M. D.; Storoni, L. C.; Read, R. J. Phaser crystallographic software. *J. Appl. Crystallogr.* **2007**, *40* (4), 658−674.
(59) Emsley, P.; Cowtan, K. Coot: model-building tools for molecular graphics. *Acta Crystallogr., Sect. D: Biol. Crystallogr.* **2004**, *60* (12), 2126−2132.
(60) Afonine, P. V.; Grosse-Kunstleve, R. W.; Echols, N.; Headd, J. J.; Moriarty, N. W.; Mustyakimov, M.; Terwilliger, T. C.; Urzhumtsev, A.; Zwart, P. H.; Adams, P. D. Towards automated crystallographic structure refinement with phenix.refine. *Acta Crystallogr., Sect. D: Biol. Crystallogr.* **2012**, *68* (4), 352−367.
(61) Joosten, R. P.; Salzemann, J.; Bloch, V.; Stockinger, H.; Berglund, A. C.; Blanchet, C.; Bongcam-Rudloff, E.; Combet, C.; Da Costa, A. L.; Deleage, G.; et al. PDB_REDO: automated re-refinement of X-ray structure models in the PDB. *J. Appl. Crystallogr.* **2009**, *42* (3), 376−384.
(62) Schuttelkopf, A. W.; van Aalten, D. M. PRODRG: a tool for high-throughput crystallography of protein-ligand complexes. *Acta Crystallogr., Sect. D: Biol. Crystallogr.* **2004**, *60* (8), 1355−1363.
(63) Krissinel, E.; Henrick, K. Inference of macromolecular assemblies from crystalline state. *J. Mol. Biol.* **2007**, *372* (3), 774−797.
(64) Sundberg, E. J.; Andersen, P. S.; Schlievert, P. M.; Karjalainen, K.; Mariuzza, R. A. Structural, energetic, and functional analysis of a protein-protein interface at distinct stages of affinity maturation. *Structure* **2003**, *11* (9), 1151−1161.
(65) Giddens, J. P.; Wang, L. X. Chemoenzymatic glyco-engineering of monoclonal antibodies. *Methods Mol. Biol.* **2015**, *1321*, 375−387.

DOI: 10.1021/acscentsci.8b00917
ACS Cent. Sci. 2019, 5, 524−538

(66) Houde, D.; Berkowitz, S. A.; Engen, J. R. The utility of hydrogen/deuterium exchange mass spectrometry in biopharmaceutical comparability studies. *J. Pharm. Sci.* **2011**, *100* (6), 2071−2086.
(67) Saphire, E. O.; Parren, P. W.; Pantophlet, R.; Zwick, M. B.; Morris, G. M.; Rudd, P. M.; Dwek, R. A.; Stanfield, R. L.; Burton, D. R.; Wilson, I. A. Crystal structure of a neutralizing human IGG against HIV-1: a template for vaccine design. *Science* **2001**, *293* (5532), 1155−1159.

DOI: 10.1021/acscentsci.8b00917
ACS Cent. Sci. 2019, 5, 524−538